The Journal of Neuroscience, November 1, 2001, *21*(21):8495–8504

Dominant-Negative Synthesis Suppression of Voltage-Gated Calcium Channel $Ca_v2.2$ Induced by Truncated Constructs

Ayesha Raghib, Federica Bertaso, Anthony Davies, Karen M. Page, Alon Meir, Yuri Bogdanov, and Annette C. Dolphin

Department of Pharmacology, University College London, London WC1E6BT, United Kingdom

Voltage-gated calcium channel $\alpha 1$ subunits consist of four domains (I–IV), each with six transmembrane segments. A number of truncated isoforms have been identified to occur as a result of alternative splicing or mutation. We have examined the functional consequences for expression of full-length $Ca_v2.2$ ($\alpha 1B$) of its coexpression with truncated constructs of $Ca_v2.2$. Domains I-II or domains III-IV, when expressed individually, together with the accessory subunits $\beta 1b$ and $\alpha 2\delta$-1, did not form functional channels. When they were coexpressed, low-density whole-cell currents and functional channels with properties similar to wild-type channels were observed. However, when domain I-II, domain III-IV, or domain I alone were coexpressed with full-length $Ca_v2.2$, they markedly suppressed its functional expression, although at the single channel level, when channels were recorded, there were no differences in their biophysical properties. Furthermore, when it was coexpressed with either domain I-II or domain I, the fluorescence of green fluorescent protein (GFP)–$Ca_v2.2$ and expression of $Ca_v2.2$ protein was almost abolished. Suppression does not involve sequestration of the $Ca_v\beta$ subunit, because loss of GFP–$Ca_v2.2$ expression also occurred in the absence of β subunit, and the effect of domain I-II or domain I could not be mimicked by the cytoplasmic I-II loop of $Ca_v2.2$. It requires transmembrane segments, because the isolated $Ca_v2.2$ N terminus did not have any effect. Our results indicate that the mechanism of suppression of $Ca_v2.2$ by truncated constructs containing domain I involves inhibition of channel synthesis, which may represent a role of endogenously expressed truncated Ca_v isoforms.

Key words: calcium channel; truncation; expression; suppression; protein synthesis; GFP

Voltage-gated calcium channels subserve a number of functions, including neurotransmitter release, regulation of gene transcription, and muscle contraction (Catterall, 2000). They are heteromeric complexes consisting minimally of three subunits, namely the pore-forming $\alpha 1$ subunit and the accessory β and $\alpha 2$-δ subunits. The $\alpha 1$ subunit is the structural and functional core of the channel and consists of four homologous domains (Dom I–IV), linked by intracellular loops and with intracellular N and C termini. Each domain contains six transmembrane-spanning segments (S1–S6). To date, 10 $\alpha 1$ subunits have been cloned and expressed (Birnbaumer et al., 1994; Perez-Reyes and Schneider, 1994; Catterall, 2000), termed $\alpha 1A$-$\alpha 1I$ and $\alpha 1S$, now renamed Ca_v1–3 (Ertel et al., 2000).

Mutations in calcium channel $\alpha 1$ subunits can contribute to a number of pathological states, and some of these mutations involve the introduction of a premature stop codon. For example, in episodic ataxia type-2 (EA-2), a number of mutations in the $Ca_v2.1$ subunit predict truncated forms of this channel (Ophoff et al., 1996; Denier et al., 1999). Most identified mutations in EA-2 introduce stop codons at the end of domain II–S6, in domain III–S1, and in the S1 segments of domains III and IV. The truncation at S1 of domain III is of particular interest because a 95 kDa protein has been identified that normally copurifies with $Ca_v2.1$ (Scott et al., 1998). This protein appears to contain domains I, II, and part of the II–III loop of $Ca_v2.1$. Thus, it is very similar to the predicted truncation in EA-2. To date, no naturally occurring two-domain splice variants of $Ca_v2.1$ that would give rise to such a two-domain protein product have been found. Recently, novel splice variants of $Ca_v1.2$ have been identified, generated by alternative splicing in the II-III loop, which predict two truncated forms of $Ca_v1.2$, consisting of domains I and II (Wielowieyski et al., 2001). In addition, a splice variant of $Ca_v2.2$ has been identified in humans and rodents that would introduce a stop codon near the end of the II-III loop (Mittman, Agnew, 2000). The expression of this splice variant would give rise to a protein consisting of domains I and II of $Ca_v2.2$. Little is known about the tissue-specificity or developmental regulation of expression of such splice variants, except that an isoform consisting of the first two domains of $Ca_v1.1$ is the main transcript in newborn muscle, whereas the four-domain isoform is predominant in adult muscle (Malouf et al., 1992). Furthermore, it has recently been found that during development of a tunicate tadpole, a truncated calcium channel with homology to $Ca_v1.1$, consisting of domains III and IV with part of domain II was expressed from a maternal transcript (Okagaki et al., 2001).

In the present study, we have examined the expression, physiological function, and effects on channel protein levels of truncations of the N-type calcium channel $Ca_v2.2$. Our results indicate that constructs containing transmembrane domain I suppress the synthesis of full-length $Ca_v2.2$.

Received June 11, 2001; revised Aug. 15, 2001; accepted Aug. 23, 2001.

This work was supported by the Wellcome Trust and Medical Research Council (MRC). A.R. was an MRC PhD student. We thank Dr. E. Perez-Reyes for $\beta 1b$ cDNA, Dr. Y. Mori for $Ca_v2.2$ cDNA, Dr. H. Chin for $\alpha 2\delta$-1 cDNA, and Dr. T Hughes for mut3-GFP cDNA. We thank Nuria Balaguero, Wendy Pratt, and Manuela Nieto-Rostro for technical assistance.

A.R. and F.B. contributed equally to this work.

Correspondence should be addressed to A. C. Dolphin, Department of Pharmacology, University College London, Gower Street, London WC1E6BT, UK. E-mail: a.dolphin@ucl.ac.uk.

MATERIALS AND METHODS

Materials. The following cDNAs were used: rat β1b (Tomlinson et al., 1993), rabbit $Ca_v2.2$ (D14157), rat α2δ-1 (M86621), and green fluorescent protein (GFP) mut3b (Cormack et al., 1996).

Truncated $Ca_v2.2$ channel constructs. Constructs containing different domains of the rabbit $Ca_v2.2$ channel were made using the PCR with primers incorporating either start or stop codons and restriction enzyme sites. The following primers were used: N-term (forward): 5′-GCG ACT AGT ATG GTC CGC TTC GGG GAC −3′ and (reverse): 5′-GTA CTC GAG CCA CTC GGT GAT GCG-3′ (introduces a stop codon at the end of the N terminus); Dom I (reverse): 5′-TTA ACT AGT TTA CTG TGC CTT CAC CAT GCG-3′ (introduces a stop codon at the end of the I-II loop); Dom I–II (reverse): 5′-CTC GAC TAG TTA CAT GGT CAC AAT GTA GTG-3′ (introduces a stop codon at the end of the II-III loop); Dom III–IV (forward): 5′-TGG CCA CTA GTA TG G ACA ACC TTG CCA ATG-3′ (introduces a start codon at the beginning of the II-III loop).

In the GFP–$Ca_v2.2$, the stop codon of GFP was removed, and GFP was fused to the N terminus of $Ca_v2.2$ by PCR. The sequence for the forward primer was 5′-*GAT GAA CTA TAC AAA* ATG GTC CGC TTC GG-3′. The sequence in italics indicates the end of GFP (with the stop codon removed), and the underlined sequence indicates the beginning of $Ca_v2.2$. GFP was fused to the Dom I–II construct using the same primer. Enhanced yellow fluorescent protein (EYFP) (Clontech, Cowley, UK) was fused onto the N terminus of the Dom I construct using the primer, 5′-*GAG CTG TAC AAG TCC GGA* ATG GTC CGC TTC GGG-3′. The sequence in italics indicates the end of EYFP, and the underlined sequence indicates the beginning of $Ca_v2.2$. For the I–II loop construct, the following primers were used: 5′-GGAGAATTCGCTATGGAGCGCGAGAGAGTG-3′ (forward with an *Eco*RI site and a start codon) and 5′-CTGTGCTCTAGACAT-GCGCCGGATG-3′ (reverse with an incorporated *Xba*I site). The resulting fragment was digested with *Eco*RI and *Xba*I enzymes and ligated in frame with the myc- and His-tags of pcDNA3.1/myc-His(+)A (Invitrogen, Paisley, UK) vector. The validity of the construct was further confirmed by Western blot, probed with anti-His antibodies (Abs) (Santa Cruz Biotechnology, Santa Cruz, CA), after expression in COS-7 cells. The sequences of all constructs were verified by automated sequencing.

Yeast two-hybrid screening. Yeast two-hybrid studies were performed using the Matchmaker Gal4 system (Clontech). The N terminus of $Ca_v2.2$ was made by PCR using a forward primer against the vector and the reverse primer: 5′ GAT CTC GAG AGG CCA CTC GGT GAT GCG 3′. This gave a product with an *Nco*I site overlapping the 5′ ATG start codon and an *Xho*I site at the 3′ end. The digested PCR product was subcloned into the *Nco*I–*Xho*I sites of pACT2 and the *Nco*I-*Sal*I sites of pAS2–1. The constructs containing the C terminus and the I-II loop were made using the following primers: C terminus: 5′ GTG ACC ATG GAC AAT TTT GAG TAC C 3′ and 5′ TAT CGA ATT CTA GCA CCG GCG GTC G 3′; I-II loop: 5′ GTA ACC ATG GCT AAG GAG CGC GAG AG 3′ and 5′ GTA GGA AAT CTG TGC CTT CAC CAT GC 3′. These PCR products, as well as the entire calcium channel β1b subunit, were subcloned into the *Nco*I–*Eco*RI sites of both pACT2 and pAS2–1. Competent yeast cells (Y190 strain) were cotransformed with both plasmids, and β-galactosidase colony-lift filter assays were performed according to the user manual (Clontech).

Cell culture and transfection. COS-7 cells were cultured as previously described (Campbell et al., 1995) and transfected using the Geneporter transfection reagent (Qbiogene, Harefield, UK). Cells were plated onto coverslips 2–3 hr before transfection. The cDNAs (all at 1 μg/ml) for $Ca_v2.2$ or truncated domain constructs (Dom I, I–II, III–IV, N terminus, or I–II loop), α2δ-1, β1b, and GFP (when used) were mixed in a ratio of 1.5 (or 3):2:1:0.2. When both $Ca_v2.2$ and truncated construct were both present, the ratios were 1.5:1.5:2:1:0.2. When particular subunits were not used, the volume was made up with water. The DNA mixture and Geneporter (6 μg and 30 μl, respectively) were each diluted in 500 μl of serum-free medium, mixed, and applied to the cells. After 3.5 hr, 1 ml of medium containing 20% serum was added to the cells, which were then incubated at 37°C for 3 d, followed by incubation at 27°C, where stated. Lactacystin (CN Biosciences, Beeston, UK) was stored at −20°C as a 3 mM stock solution in dimethylsulfoxide (DMSO) and, when used, was added to the transfected cells at 30 μM.

Immunocytochemistry and confocal microscopy. COS-7 cells were washed twice in Tris-buffered saline (TBS; 154 mM NaCl, 20 mM Tris, pH 7.4), then fixed in 4% paraformaldehyde in TBS as described (Brice et al., 1997). The cells were permeabilized in 0.02% Triton X-100 and incubated with blocking solution [20% (v/v) goat serum, 4% (w/v) bovine serum albumin (BSA), and 0.1% D,L-lysine in TBS]. In experiments using mouse monoclonal anti-GFP Ab (Clontech), or anti-myc Ab (9E10; Santa Cruz), they were used at 20 and 0.4 μg/ml, respectively, and the secondary Ab was 10 μg/ml goat anti-mouse IgG conjugated to Texas Red (Molecular Probes, Eugene, OR). In some experiments, cells were incubated for 20 min with Texas Red phalloidin (6.6 μM; Molecular Probes). The nuclear dye 4′,6-diamidino-2-phenylindole (DAPI; 300 nM; Molecular Probes) was also used to visualize the nucleus. Cells were then washed in TBS five times for 5 min each. Coverslips were mounted directly onto a microscope slide with Vectorshield (Vector Laboratories, Burlingame, CA), and the cells were examined on a laser-scanning confocal microscope (Leica TCS SP; Leica, Milton Keynes, UK). The optical sections were 0.2 μm, and all images were scanned sequentially to eliminate cross-talk. For the immunocytochemistry experiments, n = number of different transfections performed, with at least two coverslips of cells analyzed per transfection condition.

Western blotting. COS-7 cells were resuspended in hypotonic buffer (10 mM Tris, pH 7.4), containing protease inhibitors (complete EDTA-free; Roche Diagnostics, Lewes, UK) and 2 mM EDTA. Aliquots were taken for assay of total lysate protein (BCA; Perbio Science, Chester, UK), and the remainder of each sample was then solubilized in SDS-PAGE sample buffer containing 2% SDS. The samples were sonicated briefly (three times for 5 sec each on ice) and then centrifuged (10,000 × *g*, 15 min, 4°C) to remove any insoluble material. Samples (50 μg of total protein/lane) were separated by SDS-PAGE using 7.5% resolving gels and then transferred electrophoretically to polyvinylidene fluoride membranes. The membranes were blocked with 3% BSA for 5 hr at 55°C and then incubated overnight at 20°C with a 1:1000 dilution of either anti-GFP monoclonal Ab, or an anti-peptide Ab raised in rabbits against residues 846–861 within the II-III loop of rabbit brain $Ca_v2.2$ and purified by affinity chromatography using the immobilized synthetic peptide. Secondary Ab (a 1:1000 dilution of goat anti-mouse IgG or goat anti-rabbit IgG horseradish peroxidase conjugate, respectively) was added, and the membranes were incubated for 1 hr. After extensive washing, bound Abs were detected using enhanced chemiluminescence (Amersham Pharmacia Biotech, Little Chalfont, UK).

Whole-cell electrophysiology. Whole-cell patch-clamp recording was performed essentially as previously described (Meir et al., 2000), with 10 mM Ba^{2+} as charge carrier. Only fluorescent cells expressing GFP were used for recording. The holding potential was −100 mV, and pulses were delivered every 10 sec. Currents were measured 10 msec after the onset of the test pulse, and the average over a 2 msec period was calculated and used for subsequent analysis. The current density–voltage (*I–V*) relationships were fitted with a modified Boltzmann equation as follows:

$$I = G_{max}(V - V_{rev})/(1 + \exp(-(V - V_{50,act})/k)),$$

where I is the current density (in picoamperes per picofarad), G_{max} is the maximum conductance (in nanosiemans per picofarad), V_{rev} is the reversal potential, $V_{50,act}$ is the midpoint voltage for current activation, and k is the slope factor. Data are expressed as mean ± SEM of the number of replicates, n. Steady-state inactivation properties were measured by applying 10 sec pulse from −120 to +10 mV in 10 mV increments, followed by a 10 msec repolarization to −100 mV before the 40 msec test pulse to +20 mV. Steady-state inactivation data were fitted with a single Boltzmann equation of the form:

$$I/I_{max} = ((A_1 - A_2)/(1 + \exp(V - V_{50,inact})/k_{inact})) + A_2,$$

where I_{max} is the maximal current, $V_{50,inact}$ is the half-maximal voltage for current inactivation, k_{inact} is the slope factor, and A_1 and A_2 represent the proportion of inactivating and noninactivating current, respectively.

Single-channel electrophysiology. Recordings were performed on GFP-positive cells at 20–24°C. Recording pipettes were pulled from borosilicate tubes (World Precision Instruments, Sarasota, FL), coated with Sylgard (Sylgard 184, Dow Corning, Wiesbaden, Germany), and fire-polished. The bath solution, designed to zero the resting membrane potential (Meir and Dolphin, 1998) was composed of (in mM): 135 K-aspartate, 1 $MgCl_2$, 5 EGTA, and 10 HEPES (titrated with KOH, pH 7.3), and the patch pipettes were filled with a solution of the following composition (in mM): 100 $BaCl_2$, 10 TEA-Cl, and 10 HEPES, with 200 nM TTX, titrated with TEA-OH to pH 7.4. Both solutions were adjusted to an osmolarity of 320 mOsmol with sucrose. Data were sampled at 10 kHz and filtered on-line at 2 kHz. (Axopatch 200B and Digidata 1200; Axon Instruments, Foster City, CA). Voltages were not corrected for

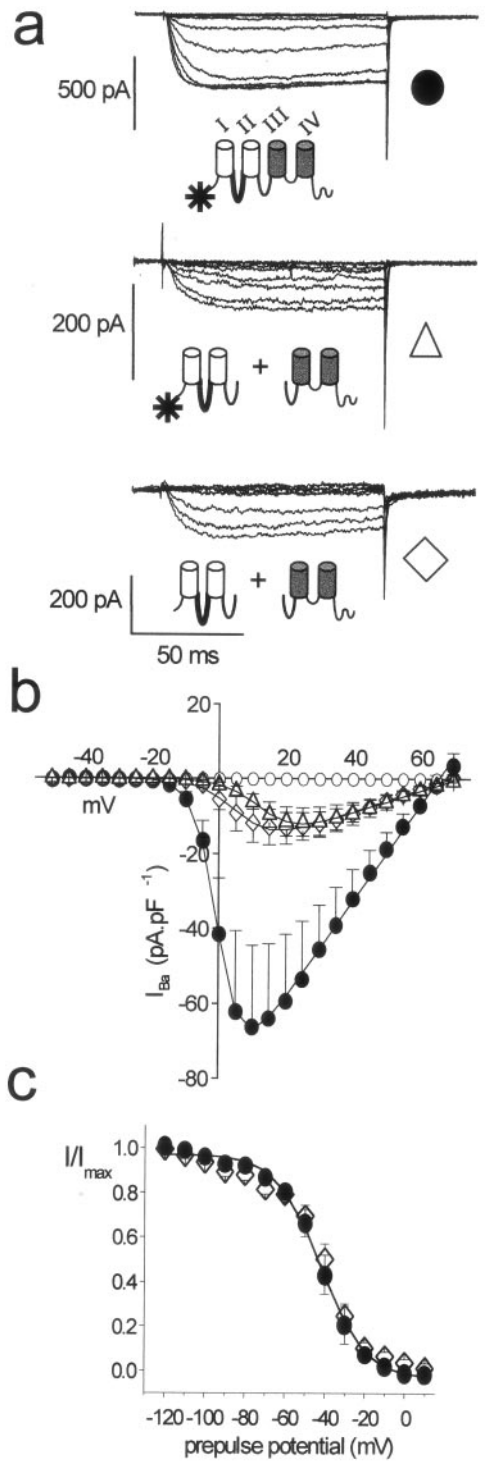

Figure 1. Functional expression of GFP-tagged $Ca_v2.2$ and formation of functional channels by coexpression of constructs consisting of Dom I–II and Dom III–IV. Cells were transfected with the constructs stated together with β1b and $\alpha2\delta$-1 cDNAs. *a,* I_{Ba} recorded from cells transfected with: GFP–$Ca_v2.2$ (*top panel*); GFP-Dom I–II and Dom III–IV (*middle panel*), and Dom I–II and Dom III–IV (*bottom panel*). Cells held at −100 mV. Test potentials −50 to +70 mV (only traces between −20 and +10 mV shown). *Asterisks* indicate GFP tag. *b,* Mean *I–V* relationships for GFP–$Ca_v2.2$ (●; $n = 10$); GFP-Dom I–II and Dom III–IV (△; $n = 6$), and Dom I–II and Dom III–IV (◇; $n = 8$);. I_{Ba} at +20 mV was −59.2 ± 17.9 pA/pF ($n = 10$) for GFP–$Ca_v2.2$ and −55.1 ± 8.3 pA/pF for untagged $Ca_v2.2$ ($n = 12$; p = NS; data not shown). The *I–V* parameters were also unaltered for both $V_{50,act}$ (+8.8 ± 1.5 mV for $Ca_v2.2$ and +3.0 ± 3.0 mV for GFP–$Ca_v2.2$; p = NS) and k (+4.4 ± 0.5 for $Ca_v2.2$ and +3.3 ± 0.5 for GFP–$Ca_v2.2$; p = NS). For untagged Dom I–II and Dom III–IV, I_{Ba} at −20 mV was −13.2 ± 4.2 pA/pF, and the *I–V* parameters were: $V_{50,act}$ = +11.5 ± 2.8 mV, k = +4.8 ± 0.6 (p = NS; compared with $Ca_v2.2$). GFP-Dom I–II plus Dom III–IV gave similar results (I_{Ba} was −11.4 ± 3.8 pA/pF) with slight shift of $V_{50,act}$ (+15.0 ± 2.0 mV; $p < 0.05$ compared with GFP–$Ca_v2.2$) and an increase in k (+5.4 ± 0.4 mV; $p < 0.01$). When either Dom I–II or Dom III–IV were expressed alone, no current was detected (○; $n = 6$). *c,* Steady-state inactivation curves for GFP–$Ca_v2.2$ (●) and Dom I–II plus Dom III–IV (◇) together with fits (*solid lines*). $V_{50,inact}$ was −38.6 ± 0.9 mV for GFP–$Ca_v2.2$ ($n = 5$) and −40.1 ± 1.3 mV for Dom I–II plus Dom III–IV ($n = 5$; p = NS), whereas k_{inact} values were +9.8 ± 0.8 and +10.9 ± 1.1, respectively (p = NS).

liquid junction potential (Neher, 1995), measured to be −15 mV in these solutions.

Leak subtraction was performed as described (Meir et al., 2000). Event detection was performed using the half-amplitude threshold method. Open time was determined by a single or double exponential fit to the open time distributions. Closed times were determined similarly using only patches with no overlapping openings. The latency to first opening was measured in 2 msec bins and analyzed as described (Meir et al., 2000). In brief, first latency histograms were accumulated and divided by the number of episodes, to represent the cumulative probability of a first latency event (P_{FL}). If necessary these were corrected for the number of channels in the patch. We considered the number of detectable simultaneously overlapping openings as representing the number of channels active in the patch (Meir et al., 2000). To strengthen this assumption we included in the latency analysis only patches with up to three simultaneously overlapping openings.

RESULTS

Expression of GFP–$Ca_v2.2$ and truncated constructs

The functional expression of $Ca_v2.2$ in COS-7 cells was investigated using N terminal GFP-fusion proteins of $Ca_v2.2$ and several truncated forms. We first examined whether the GFP-tagged $Ca_v2.2$, expressed in combination with the accessory subunits β1b and $\alpha2\delta$-1, was able to reproduce the biophysical properties of wild-type $Ca_v2.2$. An example of a whole-cell recording of I_{Ba} from COS-7 cells transfected with GFP–$Ca_v2.2$ cDNA is shown in Figure 1*a* (*top panel*), together with the voltage protocol used. The *I–V* relationship for the GFP-tagged $Ca_v2.2$ is shown in Figure 1*b* (*filled circles*). The GFP tag on the N terminus did not interfere with the functionality of the channel, because the current density at +20 mV was −55.1 ± 8.3 pA/pF for the untagged $Ca_v2.2$ channel ($n = 12$; data not shown), not significantly different from the GFP–$Ca_v2.2$ channel (−59.2 ± 17.9 pA/pF; $n = 10$). Similarly, there were no differences in other parameters of the *I–V* relationship (see legend to Fig. 1).

GFP-Dom I–II, containing only the first two domains and the intracellular II-III loop of $Ca_v2.2$, when expressed with β1b and $\alpha2\delta$-1, did not elicit any detectable currents (Fig. 1*b, open circles*). The same was true for Dom III–IV, indicating that the hemichannels are unable to form functional channels alone. In contrast, coexpression of the two hemichannels (either with or without a GFP tag on Dom I–II) resulted in the reproducible expression of small whole-cell currents, with properties otherwise analogous to the native $Ca_v2.2$ (Fig. 1*a, middle* and *bottom panels*). In cells expressing untagged Dom I–II and Dom III–IV, a +20 mV step elicited a current of −13.2 ± 4.2 pA/pF ($n = 8$). Coexpression of the GFP-Dom I–II with Dom III–IV resulted in the expression of currents with similar amplitude at +20 mV (−11.4 ± 3.8 pA/pF; $n = 7$). In addition, the steady-state inactivation properties of the reconstituted channel composed of Dom I–II and Dom III–IV did not differ from those of GFP–$Ca_v2.2$ (Fig. 1*c*).

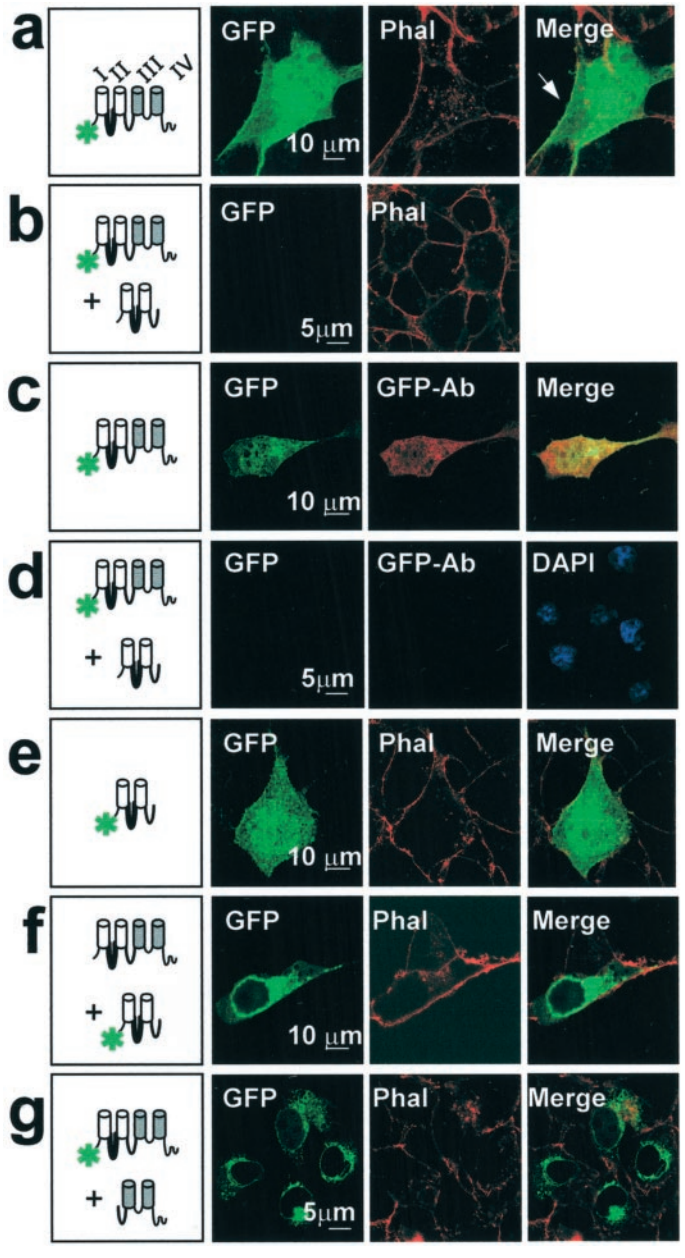

Figure 2. Expression of GFP-tagged $Ca_v2.2$ together with Dom I–II or Dom III–IV. Cells were transfected with: GFP–$Ca_v2.2$ (*a*), GFP–$Ca_v2.2$ and Dom I–II (*b*), GFP–$Ca_v2.2$ (*c*), GFP–$Ca_v2.2$ and Dom I–II (*d*); GFP–Dom I–II (*e*); $Ca_v2.2$ and GFP–Dom I–II (*f*); and GFP–$Ca_v2.2$ and Dom III–IV (*g*), as depicted in the *diagrams* on the *left*. All cells were cotransfected with β1b and α2δ-1. The *left panel* shows GFP fluorescence, the *middle panel* shows either Texas Red phalloidin (*Phal*) staining or immunolocalization of GFP using anti-GFP Ab, and the *right panel* shows either the merged image (colocalization indicated by *yellow*) or DAPI staining of the nucleus (*blue*), as stated. *Arrow* in *a* indicates colocalization of phalloidin staining and GFP–$Ca_v2.2$ at the plasma membrane.

Once the functional integrity of the GFP-tagged channel and hemichannels was proven, the expression of these fusion proteins was examined using confocal microscopy. Figure 2*a* shows the localization of GFP–$Ca_v2.2$. This subunit was expressed throughout the cell (Fig. 2*a, left panel*) ($n > 10$). The cells were also stained with Texas Red phalloidin to visualize cortical actin, which delineates the plasma membrane (Fig. 2*a, middle panel*). The yellow color in the merged image (arrow) indicates that GFP–$Ca_v2.2$ and Texas Red phalloidin are colocalized at the plasma membrane (Fig. 2*a, right panel*), in accordance with the electrophysiological results.

Effect of coexpression of two domain constructs on $Ca_v2.2$ localization

Having determined the distribution of full-length GFP–$Ca_v2.2$, we next investigated the effect of Dom I–II or Dom III–IV on the expression of GFP–$Ca_v2.2$. As shown in Figure 2*b*, untagged Dom I–II strongly suppressed the expression of GFP–$Ca_v2.2$ ($n = 6$). This was evidenced by the complete absence of observable GFP-positive cells. This could be attributable to a low level of expression, below the detection capability of the imaging system. Thus, an anti-GFP Ab was used to amplify the signal of any expressed GFP–$Ca_v2.2$ within the cells. The anti-GFP Ab was able to detect GFP–$Ca_v2.2$ alone (Fig. 2*c*) ($n = 4$), but no staining was detectable when GFP–$Ca_v2.2$ was coexpressed with Dom I–II (Fig. 2*d, center panel*) ($n = 4$). In this case, the presence of viable cells was established by using the nuclear stain DAPI (Fig. 2*d, right panel*). These results confirm that Dom I–II greatly reduces the expression of GFP–$Ca_v2.2$.

When GFP-Dom I–II was expressed alone, it was detectable at the plasma membrane and throughout the cell (Fig. 2*e, right panel*). The subcellular localization of GFP-Dom I–II was identical to that of GFP–$Ca_v2.2$ ($n > 10$). Interestingly, in the converse of the coexpression study described above, the expression of GFP-Dom I–II was not detectably reduced by the presence of untagged $Ca_v2.2$ (Fig. 2*f*).

The coexpression of GFP-Dom I–II with Dom III–IV did not alter the GFP expression or localization of GFP-Dom I–II (results not shown; $n = 6$). In contrast, coexpression of GFP–$Ca_v2.2$ with Dom III–IV altered the expression of GFP–$Ca_v2.2$ within individual cells, but did not entirely suppress it (Fig. 2*g*) ($n = 6$). In this case, GFP–$Ca_v2.2$ showed a perinuclear localization and was not readily detectable throughout the cytoplasm or at the plasma membrane by confocal microscopy (Fig. 2*g*).

Functional effects of coexpression of two-domain constructs with $Ca_v2.2$

Although immunofluorescence studies indicated that Dom I–II completely suppressed the expression of GFP–$Ca_v2.2$, it was plausible that small amounts of GFP–$Ca_v2.2$ were still expressed. This was confirmed by whole-cell recording, which showed that there was a marked reduction in I_{Ba} current density in cells expressing GFP–$Ca_v2.2$ together with either Dom I–II or Dom III–IV (Fig. 3*a*), although the *I–V* parameters were unchanged (Fig. 3*b*). I_{Ba} at +20 mV was −59.2 ± 17.9 pA/pF for GFP–$Ca_v2.2$, and was reduced to −19.2 ± 3.6 pA/pF when GFP–$Ca_v2.2$ was coexpressed with Dom I–II (67% reduction; $n = 26$; $p < 0.001$) and −18.1 ± 6.1 pA/pF with Dom III–IV (69% reduction; $n = 12$; $p < 0.001$). The steady-state inactivation parameters for $Ca_v2.2$ were also unchanged by coexpression with Dom I–II (Fig. 3*c*). Because of the suppression effect, it was necessary to coexpress free GFP, to facilitate the identification of successfully transfected cells. This did not alter the amplitude of control $Ca_v2.2$ currents (data not shown). We also examined whether the effect of Dom I–II was a nonspecific result of coexpressing another transmembrane protein, but no reduction in I_{Ba} was observed when $Ca_v2.2$ was coexpressed with the α2A-adrenergic receptor under the same conditions (I_{Ba} = −80.1 ± 24.1 pA/pF at +20 mV; $n = 6$). We further assessed whether the decrease in $Ca_v2.2$ current amplitude when it was coexpressed with Dom I–II could be a result of an alteration of the ratio

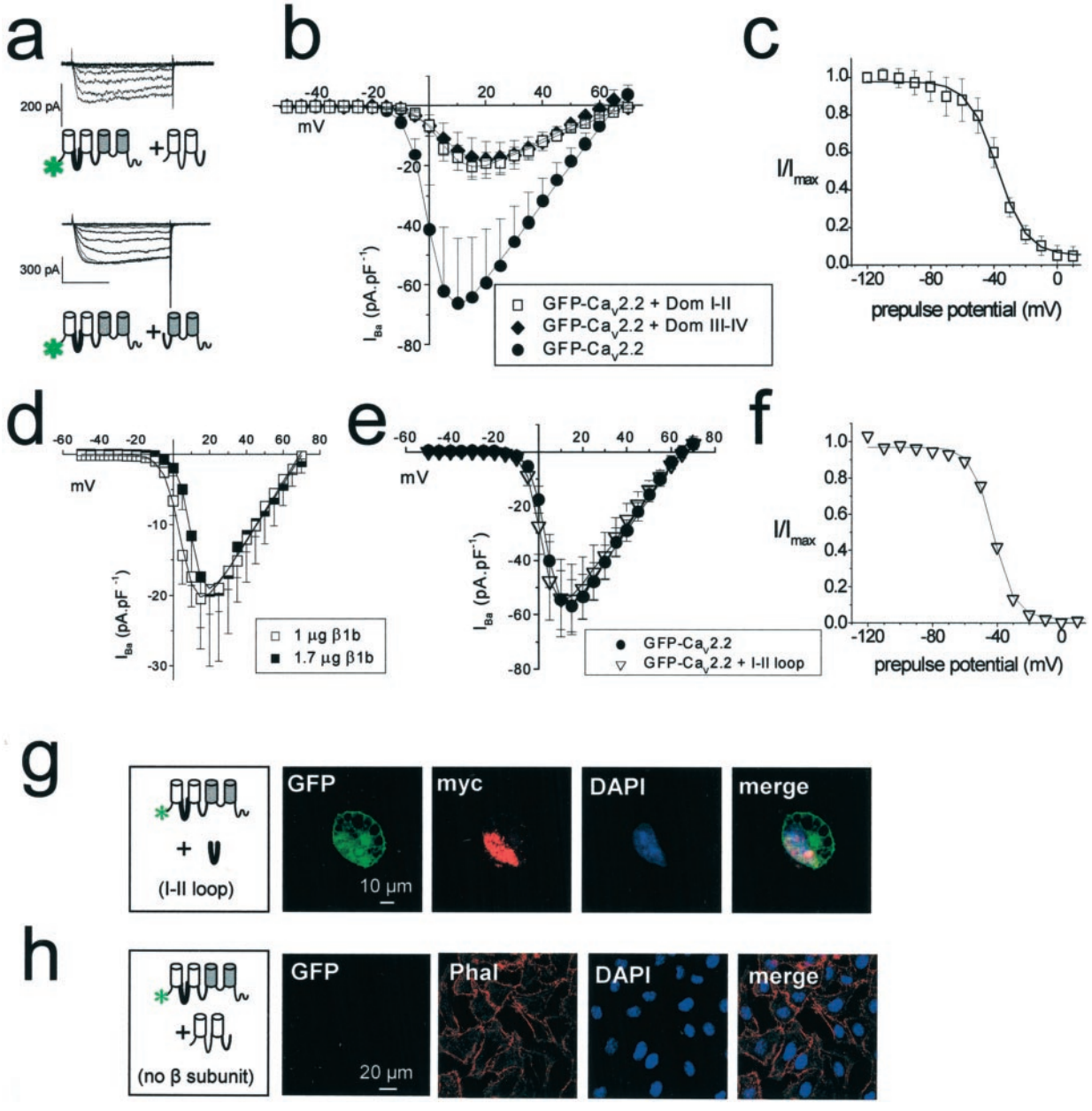

Figure 3. Functional expression of GFP-tagged $Ca_v2.2$ together with constructs consisting of Dom I–II or Dom III–IV. Cells were transfected with the cDNA constructs stated. *a,* Example traces for GFP–$Ca_v2.2$ with either Dom I–II (*top*) or Dom III–IV (*bottom*). *Asterisks* indicate GFP tag. Traces recorded between −20 and +10 mV are shown. *b, I–V* relationships for expression of GFP–$Ca_v2.2$ alone (●) or with Dom I–II (□) or Dom III–IV (♦). I_{Ba} at +20 mV was −19.2 ± 3.6 pA/pF for GFP–$Ca_v2.2$ plus Dom I–II ($n = 26$; $p < 0.001$; compared with control) and −18.1 ± 6.1 pA/pF for GFP–$Ca_v2.2$ plus Dom III–IV ($n = 12$; $p < 0.001$). The respective $V_{50,act}$ = +5.2 ± 0.3 mV and + 7.7 ± 0.8 mV. Controls (●; $n = 10$) are the same as for Figure 1 because the experiments were all performed in parallel. *c,* Steady-state inactivation for GFP–$Ca_v2.2$ plus Dom I–II. $V_{50,inact}$ = −37.8 ± 0.8 mV; k_{inact} = +9.2 ± 0.7; $n = 6$; p = NS compared with GFP–$Ca_v2.2$ (Fig. 1). *d,* Effect of transfection of different amounts (the standard amount, 1 μg, □; or 1.7 μg/dish, ■) of β1b cDNA on I_{Ba} for GFP–$Ca_v2.2$ plus Dom I–II. When using 1.7 μg β1b cDNA, I_{Ba} was −19.4 ± 10.7 at +20 mV, and $V_{50,act}$ was +10.3 ± 0.3 mV, ($n = 8$). *e, I–V* relationships for $Ca_v2.2$ alone (●; $n = 9$) or plus myc-tagged I-II loop (▽; $n = 11$). For the controls, I_{Ba} at +20 mV was −53.5 ± 8.5 pA/pF, and $V_{50,act}$ was +6.2 ± 1.5 mV. For cells coexpressing the I–II loop, I_{Ba} at +20 mV was −50.3 ± 11.4 pA/pF, and $V_{50,act}$ was +5.1 ± 1.4 mV. *f,* Steady-state inactivation of I_{Ba} in cells coexpressing GFP–$Ca_v2.2$ and I–II loop; $V_{50,inact}$ = −42.3 ± 1.5 mV; k_{inact} = +6.9 ± 0.7; $n = 5$; p = NS compared with GFP–$Ca_v2.2$. *g,* Cells transfected with GFP–$Ca_v2.2$ and myc-tagged I-II loop and cotransfected with β1b and α2δ-1. *GFP*, GFP fluorescence; *myc,* immunolocalization of myc-I-II loop using anti-myc Ab; *DAPI,* DAPI staining of the nucleus; and *merge,* merged images. *h,* Cells transfected with GFP–$Ca_v2.2$ and Dom I–II, in the absence of α2δ-1 or β1b. *GFP*, Lack of GFP fluorescence; *Phal*, Texas Red phalloidin staining; *DAPI*, DAPI staining of the nuclei; *merge*, merged images.

between the $Ca_v2.2$ and truncated construct cDNAs transfected. Therefore I_{Ba} was examined in cells transfected with half of the normal amount of GFP–$Ca_v2.2$-pMT2 cDNA (1.5 μg/dish), with the same amount of accessory subunits. No reduction in current amplitude or alteration in *I–V* parameters were detected (data not shown), indicating that the $Ca_v2.2$ cDNA amount was saturating, consistent with the fact that COS-7 cells are SV40 transformed, and the vector pMT2 contains the SV40 origin of replication. We

consistently observed that, within the range examined, reduction of the $\alpha 1$ subunit cDNA level decreased the number of cells transfected but not the current density.

To address the mechanism of suppression, we examined whether the suppressive effect of Dom I–II or Dom III–IV on $Ca_v2.2$ currents could be reduced by coexpression of both hemichannels together with $Ca_v2.2$, a result that might be predicted because our initial studies showed that Dom I–II and Dom III–IV were able to interact together to form functional channels. A protective effect was confirmed, because the I_{Ba} current density at +20 mV in cells expressing GFP–$Ca_v2.2$ together with both Dom I–II and Dom III–IV was -44.4 ± 11.9 pA/pF ($n = 9$), a nonsignificant 17% reduction ($p = 0.54$), compared with -53.5 ± 8.1 pA/pF^{-1} ($n = 9$) for control GFP–$Ca_v2.2$ currents (same controls as in Fig. 3*e*, because experiments performed in parallel).

We next examined whether the mechanism of suppression involved an accelerated degradation of $Ca_v2.2$, by examining the effect of the 26 S proteasome inhibitor lactacystin. When incubated with cells, at 30 μM, either for the entire period between transfection and visualization of GFP–$Ca_v2.2$, or for the final 16 hr, lactacystin did not increase GFP fluorescence of GFP–$Ca_v2.2$ coexpressed with Dom I–II (compared with controls receiving the same amount of solvent, $n = 6$, results not shown).

Is the suppression of expression of GFP–$Ca_v2.2$ caused by sequestration of β subunits by the truncated constructs?

The $Ca_v\beta$ subunits have been shown to act as chaperone proteins for the calcium channel $\alpha 1$ subunits, enhancing their translocation from the endoplasmic reticulum to the plasma membrane (Bichet et al., 2000). One possible explanation for the suppression of $Ca_v2.2$ currents is that Dom I–II acts to sequester free $\beta 1$b via its I-II loop, and therefore limits the amount available for chaperoning GFP–$Ca_v2.2$ to the membrane. To test this hypothesis, cells were transfected with increased $\beta 1$b cDNA, but this did not enhance $Ca_v2.2$ I_{Ba} recorded in the presence of Dom I–II (Fig. 3*d*) (I_{Ba} current density at +20 mV was -19.4 ± 10.7 pA/pF; $n = 8$). To examine further whether the effect of Dom I–II on GFP–$Ca_v2.2$ was attributable to scavenging of $\beta 1$b by the I-II loop within Dom I–II, we also coexpressed GFP–$Ca_v2.2$ with a construct of the $Ca_v2.2$ I-II loop, which we have shown to be capable of binding $\beta 1$b (Bell et al., 2001). No inhibitory effect was observed (Fig. 3*e*); the I_{Ba} current density at +20 mV in cells expressing GFP–$Ca_v2.2$ together with the free I-II loop was -50.3 ± 11.4 pA/pF ($n = 11$), a nonsignificant 5% reduction, compared with -53.5 ± 8.1 pA/pF ($n = 9$) for GFP–$Ca_v2.2$ currents recorded in parallel, from the same transfections. The steady-state inactivation parameters for GFP–$Ca_v2.2$ were also unchanged by coexpression with Dom I–II (Fig. 3*f*). In agreement with this, we saw no reduction of GFP–$Ca_v2.2$ fluorescence when it was coexpressed with the I-II loop, either in the presence or absence of coexpressed $\beta 1$b (Fig. 3*g*) (data not shown; $n = 2$). Furthermore, omission of both coexpressed accessory subunits ($\beta 1$b and $\alpha 2\delta$-1) did not affect the ability of Dom I–II to suppress expression of GFP–$Ca_v2.2$, as determined by its fluorescence (Fig. 3*h*) ($n = 6$). Because there is very low functional expression of $Ca_v2.2$ channels in the absence of these accessory subunits (Meir et al., 2000), it was not possible to perform the corresponding electrophysiological experiments.

In yeast two-hybrid experiments, we observed no interaction of $\beta 1$b with the intracellular N terminus or the C terminus of $Ca_v2.2$ ($n = 3$). In every experiment, an interaction of $\beta 1$b with a I-II loop construct was obtained as a positive control (results not shown). This rules out $\beta 1$b subunit scavenging as a mechanism of action of Dom III–IV, which contains the C terminus, but not the I-II loop.

Single channel properties of two domain constructs coexpressed together or with $Ca_v2.2$

These experiments were performed to determine whether the small whole-cell currents obtained either when Dom I–II was coexpressed with Dom III–IV or when Dom I–II was coexpressed with $Ca_v2.2$ were caused by altered properties of the channels formed. Single channels were recorded in the cell-attached mode of the patch clamp technique. The recordings were made from COS-7 cells transfected with GFP–$Ca_v2.2$ alone (Fig. 4*a*), Dom I–II together with Dom III–IV (Fig. 4*b*), or GFP–$Ca_v2.2$ with Dom I–II (Fig. 4*c*). In all cases we could detect single channels with a similar mean conductance (Fig. 4*d*), mean open time (Fig. 4*e*), mean closed time (Fig. 4*f*), and latency to first opening (Fig. 4*g*; shown at +30 mV). These values are very similar to those obtained from wild-type $Ca_v2.2$ (not tagged with GFP) (Meir et al., 2000).

Effect of coexpression of Dom I or the cytoplasmic N terminus on $Ca_v2.2$ expression

We next investigated the minimal domain required for suppression of $Ca_v2.2$ expression. To this end, GFP–$Ca_v2.2$ was coexpressed with either Dom I or the cytoplasmic N terminus of $Ca_v2.2$. The Dom I construct consisted of the intracellular N terminus, domain I, and the intracellular I-II loop. Immunofluorescence studies using YFP-Dom I confirmed its expression throughout COS-7 cells (results not shown). In a similar manner to Dom I–II, untagged Dom I also appeared to abolish the expression of GFP–$Ca_v2.2$, as assessed by confocal microscopy (Fig. 5*a*) ($n = 4$). These results were confirmed by using the anti-GFP Ab, which did not reveal any GFP–$Ca_v2.2$ (Fig. 5*b*) ($n = 4$). Again, this suppression was not affected by the absence of accessory subunits (results not shown; $n = 4$). In contrast, the N terminus of $Ca_v2.2$ did not have any effect on the expression of GFP–$Ca_v2.2$ or on its subcellular localization (Fig. 5*c*) ($n = 4$). GFP–$Ca_v2.2$ was localized at the plasma membrane (colocalized with phalloidin) and throughout the cytoplasm. In confirmation of these results, I_{Ba} recorded from cells expressing GFP–$Ca_v2.2$ and Dom I was dramatically reduced, compared with controls (Fig. 5*d*). I_{Ba} at +20 mV was -5.2 ± 1.9 pA/pF (88.4% reduction compared with control; $n = 8$). In contrast, the *I–V* parameters for cells expressing GFP–$Ca_v2.2$ together with the N terminus did not show any decrease in current amplitude or effect on activation (Fig. 5*d*). The steady-state inactivation parameters were also identical to those of GFP–$Ca_v2.2$ (Fig. 5*e*). This is in agreement with the lack of interaction observed between the $\beta 1$b subunit and the N terminus of $Ca_v2.2$ in the yeast two-hybrid assay.

Effect of coexpression of truncated constructs on the $Ca_v2.2$ protein level

The GFP–$Ca_v2.2$ expressed alone was detectable by Western blotting using either an anti-GFP Ab or an Ab against the II-III loop of $Ca_v2.2$ (band at ~250 kDa) (Fig. 6*a,b, lane 1*). A minor band at 100 kDa was also observed with both Abs, which might therefore represent an N terminal degradation product of $Ca_v2.2$. When Dom I–II was expressed alone it was detected by anti-$Ca_v2.2$, but not anti-GFP Abs (band at 120 kDa in Fig. 6*b* but not

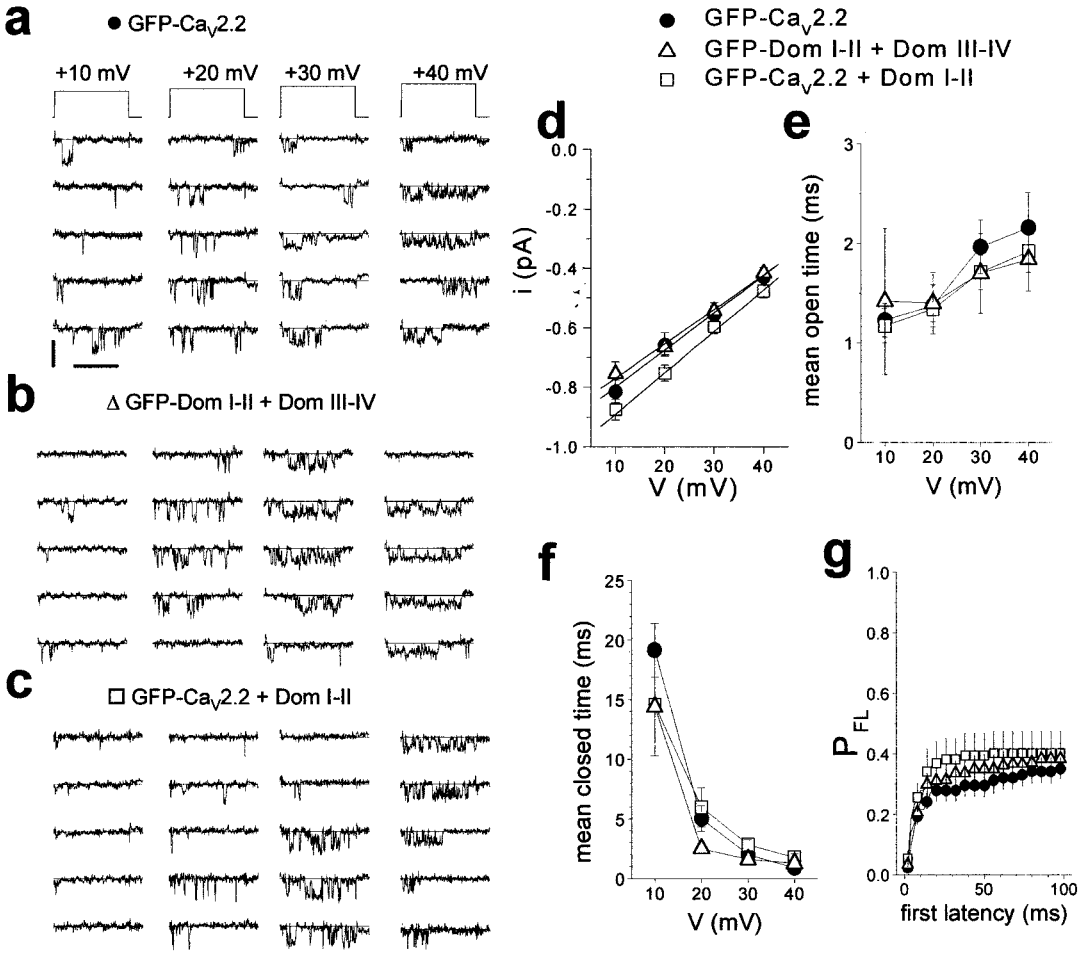

Figure 4. Properties of single channels formed by $Ca_v2.2$ compared with coexpression of Dom I–II and Dom III–IV, and coexpression of $Ca_v2.2$ with Dom I–II. Recordings were obtained from cell-attached patches from cells transfected with the stated $\alpha 1$ subunit or truncated constructs, together with $\alpha 2\delta$-1 and β1b. *a,* Single channel activity of GFP–$Ca_v2.2$. *Top,* Voltage protocol: holding potential of −100 mV, test potential to the indicated value for 100 msec. Steps were delivered every 5 sec. Five representative patch current traces (in a patch with no overlapping openings), for the voltage indicated above each column. The zero current line that runs through the traces, represents the closed state, and openings are downward deflections. Calibration: 1 pA, 50 msec (applies to all the voltages). *b,* Single-channel activity (in a patch with no overlapping openings) arising from GFP–Dom I–II coexpressed with Dom III–IV (format as in *a*). *c,* Single-channel activity from a cell transfected with GFP–$Ca_v2.2$ and Dom I–II (in a patch with no overlapping openings, format as in *a*). *d–g,* The symbols used represent the transfection conditions described in *a* (●; GFP–$Ca_v2.2$), *b* (Δ; GFP-Dom I–II and Dom III–IV), and *c* (□; GFP–$Ca_v2.2$ and Dom I–II). *d,* Unitary *I–V* relationships for the three conditions (●; n= 10), (Δ; n = 5), and (□; n = 11). These were fit by linear regression (the lines here are the average fit in each condition). The single channel conductance was 12.6 ± 1.0, 11.6 ± 1.2, and 13.8 ± 1.0 pS for the three conditions, respectively. *e,* Voltage dependence of mean channel open times (see Materials and Methods) for the three conditions (●; n = 8), (Δ; n = 5), and (□; n = 11). *f,* Voltage dependence of mean channel closed times for the three conditions (●; n = 2), (Δ; n = 1), and (□; n = 5). *g,* Latency to first opening (see Materials and Methods) in response to +30 mV test pulse for the three conditions (●; n = 4), (Δ; n = 5), and (□; n = 4).

Fig. 6*a, lane 2*). However, when GFP–$Ca_v2.2$ was expressed together with Dom I–II, no band at 250 kDa was observed with either Ab (Fig. 6*a,b*, *lane 3*), although Dom I–II was detected by the anti-$Ca_v2.2$ Ab, to a similar level as when it was expressed alone (Fig. 6*b*, compare *lanes 2* and 3). This is in agreement with the confocal imaging data (Fig. 2). No smaller molecular weight (MW) bands that might represent partially synthesized or degradation products of GFP–$Ca_v2.2$ were observed when it was cotransfected with Dom I–II, using either Ab (Fig. 6*a,b*, *lane 3*). Neither the 250 and 120 kDa bands nor the 100 kDa putative proteolytic product of GFP–$Ca_v2.2$ were present in nontransfected cells (Fig. 6*a,b*, *lane 4*). Similar results were obtained when GFP–$Ca_v2.2$ was expressed together with GFP-Dom I–II or Dom I (results not shown). In contrast, in the case of coexpression of GFP–$Ca_v2.2$ with Dom III–IV, there was little, if any, reduction in the amount of GFP–$Ca_v2.2$ (Fig. 6*c*, compare *lanes 1* and 3), in agreement with the confocal imaging data (Fig. 2*g*).

DISCUSSION

It has been suggested that four-domain Na^+ and Ca^{2+} channels arose during evolution from two sequential gene duplications of a K^+ channel (Plummer et al., 1997) and that expression of the two-domain isoforms still occurs in a developmentally regulated manner (Plummer et al., 1997). It is possible that the two-domain isoforms of $Ca_v1.1$, $Ca_v1.2$, and the Na^+ channel SCN8A may all serve a similar function (Plummer et al., 1997). It would be predicted from our results that this would be a dominant-negative function, to suppress expression of the full-length channel. In support of this, a three-domain construct of an ascidian calcium channel, thought to be expressed from maternal transcript, has

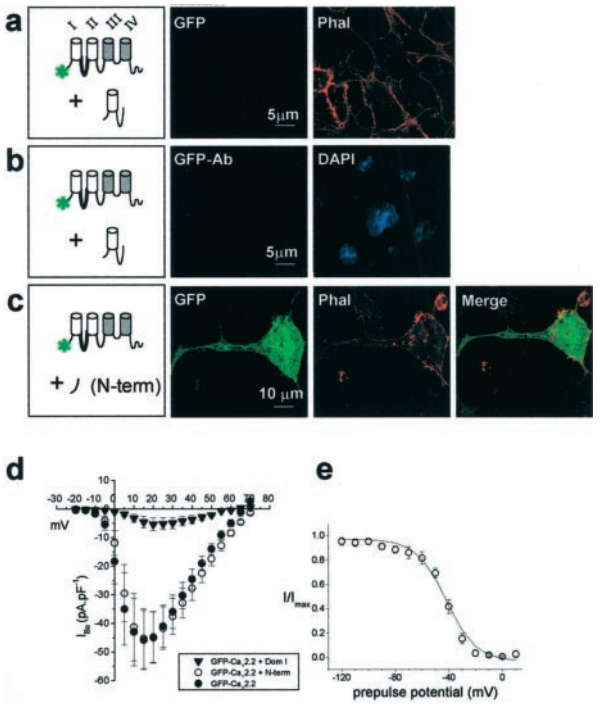

Figure 5. Effect of coexpression of Dom I or the intracellular N terminus of $Ca_v2.2$ on $Ca_v2.2$ expression and function. All cells were transfected with the constructs stated and β1b and $\alpha2\delta$-1 accessory subunit cDNAs. *a, b,* GFP–$Ca_v2.2$ and Dom I; *c,* GFP–$Ca_v2.2$ and the N terminus of $Ca_v2.2$. *Left panel* shows GFP fluorescence or immunolocalization of GFP using anti-GFP Ab; *middle panel* shows either Texas Red phalloidin or DAPI, and *right panel* shows the merged image, as stated. *d, I–V* relationships for GFP–$Ca_v2.2$ alone (●, $n = 7$; $I_{Ba} = -44.8 \pm 8.9$ pA/pF at +20 mV; $V_{50,act} = +6.4 \pm 2.1$ mV); GFP–$Ca_v2.2$ plus N terminus (○, $n = 11$; $I_{Ba} = -44.9 \pm 8.6$ pA/pF at +20 mV; $V_{50,act} = +8.9 \pm 1.8$ mV; p = NS) or GFP–$Ca_v2.2$ plus Dom I (▼, $n = 8$; $I_{Ba} = -5.2 \pm 1.9$ pA/pF at +20 mV; $V_{50,act} = +14.7 \pm 1.5$ mV; both $p < 0.001$ compared with control). *e*, Steady-state inactivation curve (fitted with a Boltzmann function, *solid line*) for GFP–$Ca_v2.2$ plus N terminus (○; $V_{50,inact} = -42.0 \pm 0.7$ mV; $k_{inact} = 7.9 \pm 0.7$; $n = 5$). Data are superimposed on the Boltzmann fit for the steady-state inactivation curve for GFP–$Ca_v2.2$ from Figure 1 for comparison (*dotted line*).

recently been shown to suppress expression of the full-length ascidian calcium channel (Okagaki et al., 2001).

Dominant-negative suppression of K^+ channel tetramer function by transmembrane fragments has been studied previously for the K_v channel family (Tu et al., 1995). This suppression effect was found to involve multiple transmembrane peptides but not to affect synthesis (Tu et al., 1996). As discussed in that study, the formation of K^+ channel tetramers will involve multiple interactions between domains, and disruption at any stage of biogenesis may be sufficient to cause suppression of functional expression (Tu et al., 1996). In contrast, another recent study showed the existence of a pathway involving arrest of synthesis and rapid degradation of mis-folded human *ether-a-go-go*-related gene (HERG) K^+ channel tetramers induced by a point mutation (Kagan et al., 2000).

Here we have examined whether the mechanism of suppression of expression of full-length $Ca_v2.2$ by truncated constructs involves (1) interference with gating of the channel inserted in the plasma membrane, (2) interference with delivery to the plasma membrane, (3) increased protein degradation, or (4) synthesis arrest. Below we consider these possibilities in turn.

Is there an impairment of gating caused by association of

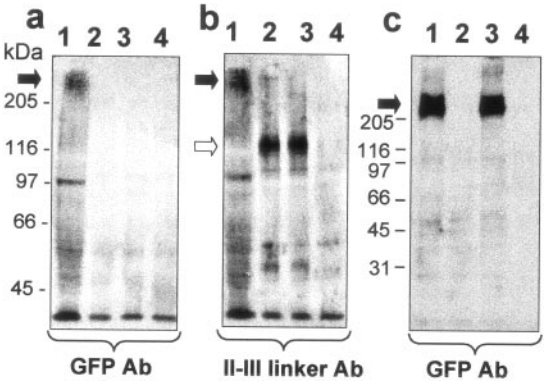

Figure 6. Effect of cotransfection of COS-7 cells with Dom I–II on the level of expressed full-length GFP–$Ca_v2.2$. Western blotting and immunodetection using (*a, c*) anti-GFP Ab (*lanes 1–4*), or anti-rabbit brain α1B II-III loop Ab (*b*, *lanes 1–4*), performed as described in Materials and Methods. *a*, *b*, *Lane 1,* GFP–$Ca_v2.2$; *lane 2,* Dom I–II; *lane 3,* GFP–$Ca_v2.2$ and Dom I–II, and *lane 4,* no transfected cDNA. Positions of molecular weight markers are shown on the left referring to both *a* and *b*. *Closed arrow* shows position of $Ca_v2.2$ band, detected with both Abs, and *open arrow* shows position of Dom I–II, only detected with anti-II-III loop Ab. Representative of four similar experiments. *c,* Lane 1: GFP–$Ca_v2.2$; *lane 2,* Dom III–IV; *lane 3,* GFP–$Ca_v2.2$ and Dom III–IV, and *lane 4,* no transfected cDNA. Positions of molecular weight markers are shown on the *left*. *Closed arrow* shows position of $Ca_v2.2$ band.

channel fragments with full-length $Ca_v2.2$ in the plasma membrane? From the electrophysiological data, GFP-Dom I–II coexpressed with Dom III–IV resulted in small but reproducible whole-cell calcium channel currents and produced single channels whose properties, apart from frequency of observation, were indistinguishable from wild type. Therefore, at least a small proportion of the truncated constructs must be able to fold and assemble together correctly with the normal topology. Similar results have recently been obtained for coexpression of two domain constructs of $Ca_v1.1$ (Ahern et al., 2001).

Concerning the mechanism of suppression, a combination of the whole-cell and single channel analysis indicates that the inhibition of full-length $Ca_v2.2$ currents by Dom I–II is attributable to a reduction in the number of channels, because there is no alteration in any of their biophysical properties examined. Although fewer $Ca_v2.2$ channels reach the plasma membrane, their gating is not modified by an association with the truncated construct. The apparent discrepancy between the confocal imaging data, where almost no GFP fluorescence was seen when Dom I–II was coexpressed with GFP–$Ca_v2.2$, and the electrophysiological data, may be a function of the detection limit, which has been calculated to be ~10,000 GFP molecules per tissue culture cell (Patterson et al., 1997). From our data, only ~3000 channels would be required to give rise to the currents observed when Dom I–II is coexpressed with GFP–$Ca_v2.2$. It is also possible that the GFP tag is synthesized, but mis-folded, and therefore not fluorescent, but it was also not recognized by the GFP Ab.

Is there interference in the delivery of the channel to the plasma membrane? $Ca_v\beta$ subunits are involved both in trafficking α1 subunits and in modulating their biophysical properties (Chien et al., 1995; Brice et al., 1997; Bichet et al., 2000; Canti et al., 2001). It is conceivable that trafficking of $Ca_v2.2$ through the endoplasmic reticulum might be compromised by scavenging of $Ca_v\beta$ subunits by the truncated fragments. However, suppression was not prevented by expression of an increased amount of β subunit. Furthermore, the properties of the currents in the pres-

ence of the truncated constructs did not mimic those of $Ca_v2.2$ expressed without β subunits in COS-7 cells or *Xenopus* oocytes, where both the V_{50} for activation and steady-state inactivation were markedly depolarized (Canti et al., 2000; Meir et al., 2000; Stephens et al., 2000). Moreover, suppression of GFP–$Ca_v2.2$ protein expression remained evident in the absence of coexpressed accessory β subunits, indicating that it occurs before trafficking out of the endoplasmic reticulum [for which $Ca_v\beta$ is required (Bichet et al., 2000)]. From yeast two-hybrid experiments we found that, of the intracellular I-II loop, the N terminus and the C terminus of $Ca_v2.2$, only the I-II loop represents a high-affinity interaction site for β1b. However, coexpression of the I-II loop with $Ca_v2.2$ did not reduce $Ca_v2.2$ I_{Ba}, again indicating that scavenging of β subunits is not responsible for the suppressive effect of Dom I and Dom I–II. The lack of effect of the I-II loop, either to reduce expression or to affect the V_{50} for activation is presumably because the β subunit is present in excess, as also demonstrated in our recent study in *Xenopus* oocytes, where the maximum effect of β3 on expression occurred at ~6 pg of β3 cDNA for 540 pg of $Ca_v2.2$ cDNA injected per oocyte (Canti et al., 2001).

Another potential mechanism of suppression would be prevention of correct folding of $Ca_v2.2$ by the truncated domains, so that endoplasmic reticulum retention signals are not masked, and the mis-folded channel is retained in the endoplasmic reticulum. Although this may be the mechanism of $Ca_v2.2$ suppression by the Dom III–IV construct, where loss of $Ca_v2.2$ protein was not observed (Figs. 2*g,* 6*c*), in the case of the truncated constructs containing domain I, instead of observing an accumulation of the GFP–$Ca_v2.2$ signal in the endoplasmic reticulum, we observed an almost complete loss of GFP–$Ca_v2.2$ fluorescence (Figs. 2*b,d*, 5*a,b*).

This points to decreased synthesis or stability of the $Ca_v2.2$ protein. In experiments to distinguish between these possibilities, we found that inhibition of proteasome activity by lactacystin did not increase the amount of GFP–$Ca_v2.2$ observed in the presence of Dom I–II, suggesting that the mechanism does not involve enhanced proteolysis, in contrast to the finding with the HERG K^+ channel mutant (Kagan et al., 2000). From these results, the most likely explanation for suppression by truncated constructs containing domain I is that synthesis of full-length $Ca_v2.2$ is arrested. Furthermore, the intracellular N terminus alone was ineffective, suggesting that suppression may occur by interaction of the nascent transmembrane segments of the first domain of $Ca_v2.2$ with Dom I of the truncated construct. Synthesis of polytopic proteins passes through a state where up to six nascent transmembrane α-helices span the endoplasmic reticulum membrane, but are not yet integrated in its lipid bilayer, associating via ionic rather than hydrophobic interactions (Borel and Simon, 1996). When the initial transmembrane α-helices of $Ca_v2.2$ are in this state, it may be that interference occurs with further synthesis of the full-length channel, because of interaction with the Dom I and Dom I–II proteins, where, in the absence of all four transmembrane domains for assembly, inappropriate residues would remain exposed. It is possible that this would effectively halt polysomal movement on each $Ca_v2.2$ mRNA. The lack of effect of the Dom III–IV construct to suppress synthesis of $Ca_v2.2$ could be attributed to the fact that synthesis and assembly of $Ca_v2.2$ is nearer completion before the interaction occurs with transmembrane segments of Dom III–IV, which then results in trapping in the endoplasmic reticulum. Furthermore, the fact that there is a reduction, rather than an increase, in suppression when Dom I–II and Dom III–IV are together coexpressed with $Ca_v2.2$, also points to the exposure of inappropriate residues on the singly expressed hemichannels as a mechanism of suppression.

In agreement with the hypothesis that synthesis of $Ca_v2.2$ is suppressed, we observed loss of full-length GFP–$Ca_v2.2$ protein, when it was coexpressed with either Dom I–II or Dom I. Furthermore, no smaller MW partially synthesized or degradation products of $Ca_v2.2$ were observed. This also points to synthesis arrest at an early stage, rather than enhanced degradation. However, although attenuation of translation is a well established aspect of the unfolded protein response that occurs when there is an accumulation of mis-folded proteins in the endoplasmic reticulum (Chevet et al., 2001), in the present case the synthesis inhibition was specific to $Ca_v2.2$, because coexpression of $Ca_v2.2$ did not appear to reduce the level of Dom I–II, and this may therefore be a novel mechanism. We are currently examining whether the $Ca_v2.2$ mRNA level is reduced, and if so, whether this is a primary event, or a consequence of synthesis inhibition.

In conclusion, it is likely that early in the process of synthesis, if $Ca_v2.2$ associates with domain I of the truncated constructs in the endoplasmic reticulum membrane, translation of the full-length $Ca_v2.2$ channel is largely prevented. This finding may generalize to all normally or pathologically occurring calcium channel splice variants that form such truncated proteins and represent a physiological mechanism for developmental or tissue-specific channel expression.

REFERENCES

Ahern CA, Arikkath J, Vallejo P, Gurnett CA, Powers PA, Campbell KP, Coronado R (2001) Intramembrane charge movements and excitation-contraction coupling expressed by two-domain fragments of the Ca^{2+} channel. Proc Natl Acad Sci USA 98:6935–6940.

Bell DC, Butcher AJ, Berrow NS, Page KM, Brust PF, Nesterova A, Stauderman KA, Seabrook GR, Nurnberg B, Dolphin AC (2001) Biophysical properties, pharmacology and modulation of human, neuronal L-type (α1D, $Ca_v1.3$) voltage-dependent calcium currents. J Neurophysiol 85:816–828.

Bichet D, Cornet V, Geib S, Carlier E, Volsen S, Hoshi T, Mori Y, De Waard M (2000) The I-II loop of the Ca^{2+} channel α1 subunit contains an endoplasmic reticulum retention signal antagonized by the β subunit. Neuron 25:177–190.

Birnbaumer L, Campbell KP, Catterall WA, Harpold MM, Hofmann F, Horne WA, Mori Y, Schwartz A, Snutch TP, Tanabe T, Tsien RW (1994) The naming of voltage-gated calcium channels. Neuron 13:505–506.

Borel AC, Simon SM (1996) Biogenesis of polytopic membrane proteins: membrane segments assemble within translocation channels prior to membrane integration. Cell 85:379–389.

Brice NL, Berrow NS, Campbell V, Page KM, Brickley K, Tedder I, Dolphin AC (1997) Importance of the different β subunits in the membrane expression of the α1A and α2 calcium channel subunits: studies using a depolarisation-sensitive α1A antibody. Eur J Neurosci 9:749–759.

Campbell V, Berrow N, Brickley K, Page K, Wade R, Dolphin AC (1995) Voltage-dependent calcium channel β-subunits in combination with alpha1 subunits have a GTPase activating effect to promote hydrolysis of GTP by G $alpha_o$ in rat frontal cortex. FEBS Lett 370:135–140.

Canti C, Bogdanov Y, Dolphin AC (2000) Interaction between G proteins and accessory β subunits in the regulation of α1B calcium channels in *Xenopus* oocytes. J Physiol (Lond) 527:419–432.

Canti C, Davies A, Berrow NS, Butcher AJ, Page KM, Dolphin AC (2001) Evidence for two concentration-dependent processes for β subunit effects on α1B calcium channels. Biophys J 81:1439–1451.

Catterall WA (2000) Structure and regulation of voltage-gated Ca^{2+} channels. Annu Rev Cell Dev Biol 16:521–555.

Chevet E, Cameron PH, Pelletier MF, Thomas DY, Bergeron JJM (2001) The endoplasmic reticulum: integration of protein folding, quality control, signaling and degradation. Curr Opin Struct Biol 11:120–124.

Chien AJ, Zhao XL, Shirokov RE, Puri TS, Chang CF, Sun D, Rios E, Hosey MM (1995) Roles of a membrane-localized β subunit in the formation and targeting of functional L-type Ca^{2+} channels. J Biol Chem 270:30036–30044.

Cormack BP, Valdivia RH, Falkow S (1996) FACS-optimized mutants of the green fluorescent protein (GFP). Gene 173:33–38.

Denier C, Ducros A, Vahedi K, Joutel A, Thierry P, Ritz A, Castelnovo G, Deonna T, Gerard P, Devoize JL, Gayou A, Perrouty B, Soisson T, Autret A, Warter JM, Vighetto A, Van Bogaert P, Alamowitch S, Roullet E, Tournier-Lasserve E (1999) High prevalence of CACNA1A truncations and broader clinical spectrum in episodic ataxia type 2. Neurology 52:1816–1821.

Ertel EA, Campbell KP, Harpold MM, Hofmann F, Mori Y, Perez-Reyes E, Schwartz A, Snutch TP, Tanabe T, Birnbaumer L, Tsien RW, Catterall WA (2000) Nomenclature of voltage-gated calcium channels. Neuron 25:533–535.

Kagan A, Yu Z, Fishman GI, McDonald TV (2000) The dominant negative LQT2 mutation A561V reduces wild-type HERG expression. J Biol Chem 275:11241–11248.

Malouf NN, McMahon DK, Hainsworth CN, Kay BK (1992) A two-motif isoform of the major calcium channel subunit in skeletal muscle. Neuron 8:899–906.

Meir A, Dolphin AC (1998) Known calcium channel $\alpha 1$ subunits can form low threshold, small conductance channels, with similarities to native T type channels. Neuron 20:341–351.

Meir A, Bell DC, Stephens GJ, Page KM, Dolphin AC (2000) Calcium channel β subunit promotes voltage-dependent modulation of $\alpha 1B$ by $G\beta\gamma$. Biophys J 79:731–746.

Mittman S, Agnew WS (2000) Three new alternative spliced exons of the calcium channel 1B subunit gene *CACNA1B*. Soc Neurosci Abstr 26:40.4

Neher E (1995) Voltage offsets in patch-clamp experiments. In: Single-channel recording (Sakmann B, Neher E, eds), pp 147–153. New York: Plenum.

Okagaki R, Izumi H, Okada T, Nagahora H, Nakajo K, Okamura Y (2001) The maternal transcript for truncated voltage-dependent Ca^{2+} channels in the ascidian embryo: a potential suppressive role in Ca^{2+} channel expression. Dev Biol 230:258–277.

Ophoff RA, Terwindt GM, Vergouwe MN, van Eijk R, Oefner PJ, Hoffman SM, Lamerdin JE, Mohrenweiser HW, Bulman DE, Ferrari M, Haan J, Lindhout D, van Ommen GJ, Hofker MH, Ferrari MD, Frants RR (1996) Familial hemiplegic migraine and episodic ataxia type-2 are caused by mutations in the Ca^{2+} channel gene CACNL1A4. Cell 87:543–552.

Patterson GH, Knobel SM, Sharif WD, Kain SR, Piston DW (1997) Use of the green fluorescent protein and its mutants in quantitative fluorescence microscopy. Biophys J 73:2782–2790.

Perez-Reyes E, Schneider T (1994) Calcium channels: structure, function, and classification. Drug Dev Res 33:295–318.

Plummer NW, McBurney MW, Meisler MH (1997) Alternative splicing of the sodium channel SCN8A predicts a truncated two-domain protein in fetal brain and non-neuronal cells. J Biol Chem 272:24008–24015.

Scott VES, Felix R, Arikkath J, Campbell KP (1998) Evidence for a 95 kDa short form of the α_{1A} subunit associated with the ω-conotoxin MVIIC receptor of the P/Q-type Ca^{2+} channels. J Neurosci 18:641–647.

Stephens GJ, Page KM, Bogdanov Y, Dolphin AC (2000) The $\alpha 1B$ calcium channel amino terminus contributes determinants for β subunit mediated voltage-dependent inactivation properties. J Physiol (Lond) 525:377–390.

Tomlinson WJ, Stea A, Bourinet E, Charnet P, Nargeot J, Snutch TP (1993) Functional properties of a neuronal class C L-type calcium channel. Neuropharmacology 32:1117–1126.

Tu L, Santarelli V, Deutsch C (1995) Truncated K+ channel DNA sequences specifically suppress lymphocyte K+ channel gene expression. Biophys J 68:147–156.

Tu LW, Santarelli V, Sheng ZF, Skach W, Pain D, Deutsch C (1996) Voltage-gated K+ channels contain multiple intersubunit association sites. J Biol Chem 271:18904–18911.

Wielowieyski PA, Wigle JT, Salih M, Hum P, Tuana BS (2001) Alternative Splicing in the Intracellular Loop Connecting Domains II and III of the α_1 Subunit of $Ca_v1.2$ Ca^{2+} Channels Predicts Two-domain Polypeptides with unique C-terminal Tails. J Biol Chem 276:1398–1406.